Nanoscale

COMMUNICATION

Cite this: *Nanoscale*, 2019, **11**, 17216

Received 24th August 2019,
Accepted 5th September 2019

DOI: 10.1039/c9nr07307h

rsc.li/nanoscale

Promoting photoluminescence quantum yields of glass-stabilized $CsPbX_3$ (X = Cl, Br, I) perovskite quantum dots through fluorine doping†

Daqin Chen, *[a,b,c] Yue Liu,[d] Changbin Yang,[a,b,c] Jiasong Zhong, *[d] Su Zhou,[d] Jiangkun Chen[a,b,c] and Hai Huang[a,b,c]

In the last few years, all-inorganic cesium lead halide ($CsPbX_3$) quantum dots have shown unprecedented radical progress for practical applications in the optoelectronic field, but they quickly decompose when exposed to air. The *in situ* growth of the $CsPbX_3$ particles inside amorphous glass can significantly improve their stability. Unfortunately, it is formidably difficult to precipitate whole-family $CsPbX_3$ from a glass matrix and their photoluminescence quantum yields require further improvement. Herein, fluoride additives were introduced into oxyhalide borosilicate glasses to break the tight glass network, which promoted the nucleation/growth of $CsPbX_3$ (X = Cl, Cl/Br, Br, Br/I and I) inside the glass. Importantly, the quantum efficiencies of glass-stabilized $CsPbBr_3$, $CsPb(Br/I)_3$ and $CsPbI_3$ reached 80%, 60% and 50%, respectively, which are the highest efficiencies reported so far. Benefiting from the effective protection of robust glass, $CsPbX_3$ quantum dots exhibited superior water resistance with more than 90% luminescence remaining after immersing them in water for 30 days, and halogen anion exchange among different $CsPbX_3$ materials was completely inhibited. Two prototype light-emitting diodes were constructed by coupling green/red and green/orange/red quantum dots with InGaN blue chips, yielding bright white light with optimal luminous efficiency of 93 lm W^{-1}, tunable color temperature of 2000–5800 K and high color rendering index of 90.

All-inorganic $CsPbX_3$ (X = Cl, Br, I) perovskite quantum dots (PQDs) have recently emerged as hot light-emitting materials because of their superior optical performances, such as a high photoluminescence quantum yield (PLQY, up to 90%), narrow full width at half maximum (FWHM, down to 12 nm), and wide color gamut.[1–6] In the past few years, they have shown unprecedented radical progress, ranging from their synthesis and structure/property optimization to practical applications in QD-LEDs, lasers, photodetectors and scintillators.[7–26] Unfortunately, colloidal $CsPbX_3$ PQDs generally suffer from poor long-term stability upon the impact of moisture, heat and light irradiation due to their low formation energy and ionic crystal features.[27,28] Recently, embedding $CsPbX_3$ PQDs in inorganic oxide glasses (PQDs@glass) *via in situ* nucleation/growth (crystallization) has been demonstrated to be a feasible strategy to improve their stability for the effective protecting role of the robust glass matrix.[29–31] SiO_2-, P_2O_5-, GeO_2- and B_2O_3-based oxyhalide glasses containing Cs^+, Pb^{2+} and X^- elements have been prepared, with subsequent heat-treatment-induced $CsPbX_3$ crystallization in a glass matrix.[32–36] However, unlike wet-chemical synthesis, the nucleation and growth of PQDs in glass are generally limited by a tight glass network, which hinders the diffusion of Cs^+, Pb^{2+} and X^- ions and impedes the highly efficient whole-family precipitation of $CsPbX_3$ PQDs. Moreover, the current PQDs@glass nanocomposites still have several shortcomings. First, the design and optimization of the glass compositions involving trial and error experimentation are complex and random. Second, it is difficult to obtain the whole-family precipitation of $CsPbX_3$ PQDs in glasses, especially $CsPbCl_3$ and $CsPbI_3$, leading to insufficient coverage of the color gamut. Third, PLQYs of the $CsPbX_3$ PQDs@glass products are still low compared with that of the corresponding colloidal PQD counterparts, especially $CsPbCl_3$, $CsPb(Br/I)_3$ and $CsPbI_3$, which make their practical applications in optoelectronic devices difficult. Recently, $CsPbCl_3$ PQDs@glass has been successfully prepared by our group, but its PLQY is too low to be measurable.[31] The highest PLQY value for $CsPbBr_3$ PQDs@glass is 81%, which has been

[a]*College of Physics and Energy, Fujian Normal University, Fujian Provincial Key Laboratory of Quantum Manipulation and New Energy Materials, Fuzhou, China. E-mail: dqchen@fjnu.edu.cn*
[b]*Fujian Provincial Collaborative Innovation Center for Optoelectronic Semiconductors and Efficient Devices, Xiamen, 361005, China*
[c]*Fujian Provincial Engineering Technology Research Center of Solar Energy Conversion and Energy Storage, Fuzhou, China*
[d]*College of Materials & Environmental Engineering, Hangzhou Dianzi University, Hangzhou, 310018, China. E-mail: jiasongzhong@hdu.edu.cn*

†Electronic supplementary information (ESI) available: Table S1, Fig. S1–S17. Experimental section, extra XRD, HAADF-STEM images, HRTEM image, PL spectra, decay curves, luminescence photographs, EL spectra and CIE diagrams. See DOI: 10.1039/c9nr07307h

realized in boron-germanium glass; however, the PLQY value for $CsPb(Br/I)_3$ red PQDs in glass is only 20% and the values for $CsPbCl_3$ and $CsPbI_3$ PQDs in glass have not been reported.[35] Pure $CsPbI_3$ PQDs@glass has been fabricated by Xiang *et al.* and its PLQY is only 4.2%.[36]

Herein, F^- dopants were introduced into oxyhalide glass to modify the network structure, which was demonstrated to be beneficial for the controllable growth of $CsPbX_3$ PQDs. As schematically illustrated in Fig. 1a, taking SiO_2 glass as a typical example, $[SiO_4]$ tetrahedra are tightly connected to each other by bridging oxygen (BO) ions and the introduced F^- ions will partially enter the network structure by breaking the Si–O bonds to produce non-bridging oxygen (NBO, Fig. 1b), which is expected to provide enough space for ionic diffusion and thus promote the precipitation of $CsPbX_3$ PQDs in glass. To reduce the glass-melting temperature, B_2O_3 and ZnO were introduced into the SiO_2 glass network in the present work, together with the perovskite components of Cs_2CO_3, PbX_2 and NaX. NH_4F was selected as the F^- source. All these raw materials were well ground and melted at 1200 °C for 15 min to produce bulky precursor glass (PG). After heat treatment at 460–580 °C for 2 h, $CsPbX_3$ PQDs were expected to be crystallized inside the glass (Fig. 1c). Without the addition of the F^- ions, the XRD patterns of the samples prepared by heat treatments at various temperatures showed no crystalline diffraction signal (Fig. 1d). As a comparison, obvious $CsPbBr_3$ diffraction peaks were detected and became intensified and narrow with the elevation of the crystallization temperature owing to the growth of PQDs (Fig. 1e). The percentage of PQDs in glass was evaluated to be 10–15% based on the ratio of the integrated area of the crystalline diffraction peaks and the total XRD pattern. All the results confirm the promoting role of the F^- additives for $CsPbX_3$ *in situ* crystallization in glass. Importantly, this strategy enabled the precipitation of the whole-family $CsPbX_3$ (X = Cl, Cl/Br, Br, Br/I, I) PQDs in glass (Fig. 1f), leading to bright and colorful luminescence covering the entire visible spectral region (Fig. 1g).

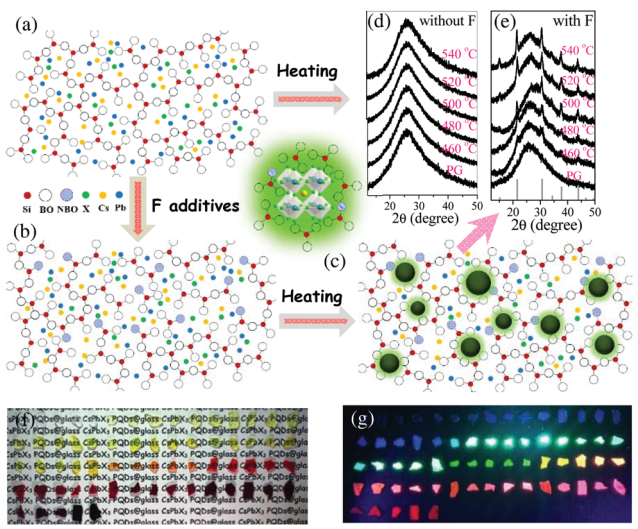

Fig. 1 Schematic illustration of F-additive-promoted $CsPbX_3$ precipitation from glass: (a, b) the proposed glass network structures without and with F additives. (c) $CsPbX_3$ crystallization in the F-added glass matrix *via* heating. (d, e) XRD patterns of glass samples heated at varied temperatures for 2 h. Bars represent standard diffraction data of cubic $CsPbBr_3$ crystal (JCPDS no. 54-0752). (f, g) A series of $CsPbX_3$ PQDs@glass monoliths under the irradiation of daylight and 365 nm UV light.

The high-angle annular dark-field (HAADF) scanning transmission electron microscopy (STEM) observation for three typical $CsPbX_3$ (X = Cl, Br, I) PQDs@glass (Fig. S1, S2,† Fig. 2a) materials showed the homogeneous distribution of PQDs in the glass matrix. The obvious contrast between $CsPbX_3$ PQDs (bright) and the glass matrix (dark) is distinctly discernible due to the large difference in the atomic numbers between Cs/Pb (Z = 55/82) and Si/B (Z = 14/5). The selected area electron diffraction (SAED) pattern (Fig. S3†) shows discrete polycrystalline diffraction rings assigned to cubic $CsPbX_3$. The high-resolution TEM (HRTEM) micrograph (Fig. S4†) confirmed the single-crystalline nature of PQDs with high crystallinity and distinctly resolved lattice fringes. As a comparison, PQDs were difficult to precipitate from the glass without F^- doping (Fig. S5†), verifying the F additive-promoted $CsPbX_3$ nucleation/growth.

A series of structural characterizations were carried out to obtain information about the glass network structure. The Fourier transform infrared (FTIR) spectra (Fig. 2b) show Si–O–Si rocking and asymmetrical vibrations at ~435 cm^{-1} and ~1030 cm^{-1}, respectively, B–O–B linkage at ~697 cm^{-1}, $[BO_3]$ vibrational structural units at ~1380 cm^{-1} and B–O stretching vibrations in the $[BO_3]$ triangles at ~1285 cm^{-1}.[37,38] The Raman spectra (Fig. 2c) evidence the existence of the $[ZnO_6]$ structural units at ~265 cm^{-1}, di-borate groups at 460 cm^{-1} and Si–O–Si bending and stretching units at 765 cm^{-1} and 1050 cm^{-1}, respectively.[38,39] All these results indicate that the glass network consists of the $[SiO_4]$, $[BO_4]$ and $[BO_3]$ units. The ^{11}B magic-angle spinning (MAS) nuclear

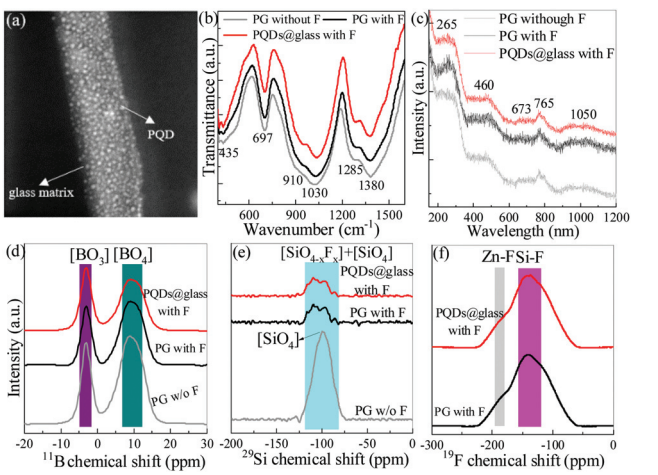

Fig. 2 (a) HAADF-STEM image of a typical $CsPbI_3$ PQDs@glass. (b) FTIR spectra, (c) Raman spectra, (d) ^{11}B, (e) ^{29}Si and (f) ^{19}F MAS-NMR spectra of precursor glasses and PQDs@glass with/without F additives.

magnetic resonance (NMR) spectra (Fig. 2d) exhibit two resonance bands at −3 ppm and 9 ppm assigned to the B^{3+} ions in the $[BO_3]$ and $[BO_4]$ units, respectively.[40] The ^{29}Si MAS-NMR spectrum for the glass without F doping showed a relatively intense and narrow resonance band at −98 ppm, which substantially weakened and broadened upon the introduction of the F^- ions (Fig. 2e). This phenomenon was attributed to the incorporation of the F^- ions into $[SiO_4]$ and the destruction of the glass network structure by breaking the Si–O bonds.[41,42] As a supplement, the ^{19}F MAS-NMR spectra (Fig. 2f) provide information on Si–F bonding, with a resonance signal at −140 ppm[41,42] for the F-doped PG and PQDs@glass nanocomposite. An extra weak resonance band at −180 ppm originated from the Zn–F bond.[43] Therefore, it can be concluded that the added F^- ions break the network structure to provide space for ionic diffusion and promote the nucleation/growth of $CsPbX_3$ PQDs in the glass. To demonstrate the versatility of the proposed doping mechanism, we extended the experimental study to doping with other fluorides. Similar to the case of NH_4F, the introduction of fluorides, namely, LiF, NaF, CaF_2, PbF_2, YF_3 and LuF_3 into glass could indeed promote the precipitation of $CsPbX_3$ NCs (Fig. S6†).

The PL spectra (Fig. 3a) evidence the tunable luminescence of $CsPbX_3$ PQDs from violet to deep red *via* the modification of the halogen types and ratios. The FWHM values were in the range of 15–52 nm and the time-resolved decays indicated their radiative lifetimes of 2–70 ns with faster emission from wider-bandgap PQDs (Fig. 3b). All these results are comparable to the cases of colloidal $CsPbX_3$ PQDs,[1,2] confirming the successful growth of PQDs in glass. Indeed, the X-ray diffraction (XRD) patterns verify that the precursor glass is amorphous and typical cubic $CsPbX_3$ (X = Cl, Br, I) diffraction peaks appear after glass crystallization (Fig. 3c). The $CsPbX_3$ PQDs@glass nanocomposites possessed a wide gamut of pure colors, as shown in the Commission International de L'Eclairage (CIE) chromaticity diagram (Fig. 3d); a selected triangle of bright blue (B), green (G) and red (R)-emitting PQDs (inset of Fig. 3d) covers up to ~200% of sRGB and ~140% of the National Television Systems Committee (NTSC) TV color standard.

In a further experiment, the influence of the crystallization temperature on the optical properties of PQDs in glass was investigated. The emission band of $CsPbCl_3$ PQDs shifted from 407 nm to 412 nm as the heat treatment temperature increased from 460 °C to 540 °C (Fig. S7a†). The precipitation of PQDs in glass was a typical diffusion-controlled process and elevating the crystallization temperature contributed to the growth and increase in the particle size, leading to the reduction in the bandgap energy of PQDs due to the quantum confinement effect and the subsequent red-shift in PL bands. As evidenced in Fig. S8–S10,† the diffraction peaks of PQDs become intensified and narrow with the increase in the crystallization temperature. Importantly, taking $CsPb(Br/I)_3$ as a typical example, increasing the crystallization temperature will not induce a shift in the diffraction peaks (Fig. S10†), indicating that the Br-to-I ratio in the precipitated $CsPb(Br/I)_3$ PQDs is stable.

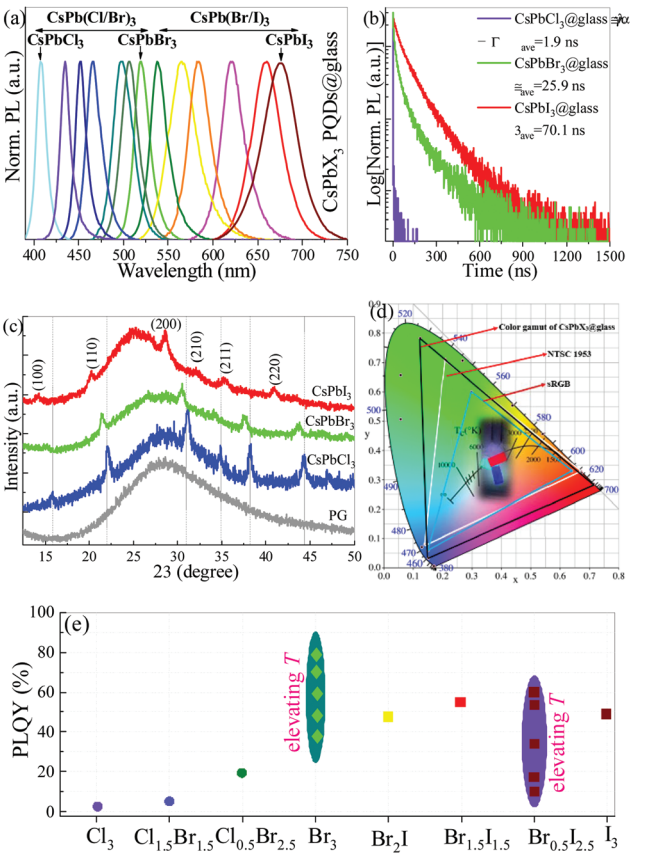

Fig. 3 (a) Representative PL spectra of $CsPbX_3$ (X = Cl, Cl/Br, Br, Br/I, I) PQDs@glass samples. (b) Time-resolved PL decays for the corresponding nanocomposites. (c) XRD patterns of PG, $CsPbCl_3$, $CsPbBr_3$ and $CsPbI_3$ PQDs@glass products. (d) Comparison of the color gamut for emission from $CsPbX_3$ PQDs@glass and two common color standards (NTSC 1953 and sRGB). Inset is the photograph of highly luminescent RGB PQDs@glass bulky materials (1.5 cm × 3.0 cm) upon the irradiation of 365 nm UV light. (e) PLQY values for the as-prepared $CsPbX_3$ (X = Cl, Cl/Br, Br, Br/I, I) PQDs@glass nanocomposites.

Certainly, for $CsPb(Cl/Br)_3$, $CsPbBr_3$, $CsPb(Br/I)_3$ and $CsPbI_3$ PQDs in glass, the PL bands exhibited similar variations with the elevation of the crystallization temperatures, *i.e.*, redshifts from 463 nm to 471 nm, 503 nm to 519 nm, 563 nm to 590 nm, and 638 nm to 688 nm, respectively (Fig. S7b–S7e†). These results confirm the ability of elaborately tuning the bandgap energies of $CsPbX_3$ PQDs in glass *via* heat treatment. Notably, the crystallization temperatures (460–540 °C) for precipitating I-containing PQDs in glass should be higher than those of Cl or Br-containing ones (500–580 °C) owing to the requirement of large activation energy for the diffusion of heavy I^- ions in glass. Furthermore, it is worth mentioning that the present glass-protected cubic $CsPbI_3$ PQDs were highly stable and could not be converted into other non-luminescent phases, which is different from the case of the colloidal cubic $CsPbI_3$ counterpart.[44]

The time-resolved decay curves show the gradual elongation of the radiative lifetime for exciton recombination with the elevation of the crystallization temperature (Fig. S7f–S7j†),

indicating the significant reduction in non-radiation de-excitation for charge carriers in PQDs. High heating temperatures are beneficial for increasing the PQD size and improving their crystallinity, which will reduce the surface defects of PQDs and improve PLQYs. Fig. 3e shows the determined PLQY values for several typical $CsPbX_3$ PQD@glass samples. For $CsPbCl_3$ and $CsPb(Cl/Br)_3$ PQDs, the PLQYs are in the range of 3%–20%; for $CsPbBr_3$ PQDs, the PLQY reaches as high as 80%; for $CsPb(Br/I)_3$ PQDs, the PLQYs are in the range of 50%–60%. Indeed, taking $CsPbBr_3$ and $CsPb(Br/I)_3$ as the typical examples, PLQY monotonously increases with the elevation of the crystallization temperature. As far as we know, this is the first report for PLQY of $CsPbCl_3$ PQDs@glass and the PLQY values of $CsPb(Br/I)_3$ and $CsPbI_3$ PQDs@glass are the highest reported so far (Table S1†).

Furthermore, the long-term stabilities of the as-prepared blue, green and red PQDs@glass samples were investigated by directly immersing them in aqueous solutions for different durations. The PL spectra show that there is no obvious change in PL intensity (Fig. 4a) and PL above 90% can be retained after immersing the nanocomposite in water for 30 days (Fig. S11†). The time-resolved spectra obtained by monitoring exciton recombination indicate that their decay kinetics

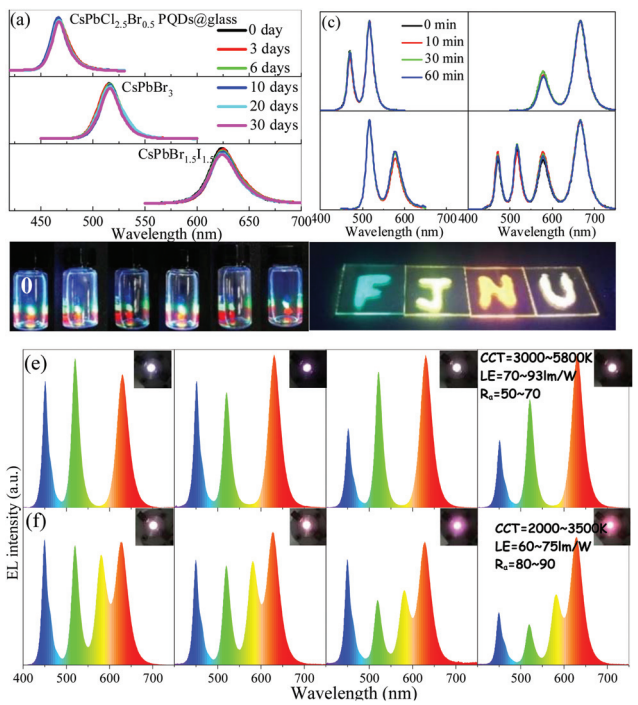

Fig. 4 Stability tests for the as-prepared $CsPbX_3$ PQDs@glass samples: (a, b) PL spectra and luminescence photographs (λ_{ex} = 365 nm) for three typical RGB PQDs directly immersed in water for 30 days. (c, d) PL spectra of the mixed $CsPbCl_{2.5}Br_{0.5}$ (460 nm), $CsPbBr_3$ (520 nm), $CsPbBr_2I$ (580 nm) and $CsPbBr_{0.5}I_{2.5}$ (660 nm) PQDs@glass powders and luminescence photographs (λ_{ex} = 365 nm) of colorful letters prepared by coating the powders on glass slides. (e, f) EL spectra of the constructed LED devices by coupling blue InGaN chips with $CsPbBr_3$/$CsPbBr_{1.5}I_{1.5}$ and $CsPbBr_3$/$CsPbBr_2I$/$CsPbBr_{1.5}I_{1.5}$ color converters; insets show the corresponding devices driven by a 100 mA operation current.

are not remarkably affected by the elongation of the storage time in water (Fig. S12†). As evidenced in Fig. 4b, the intense RGB emissions from the three typical $CsPbX_3$ (X = Cl/Br, Br, Br/I) PQDs@glass nanocomposites in water are retained over a period of 30 days. Therefore, it can be concluded that the inorganic glass host is indeed beneficial for efficiently protecting PQDs from decomposition by water. Furthermore, we demonstrated that the detrimental halogen anion exchange among different PQDs can be completely prohibited (Fig. 4c and d). Blue-emitting (460 nm) $CsPbCl_{2.5}Br_{0.5}$, green-emitting (520 nm) $CsPbBr_3$, orange-emitting (580 nm) $CsPbBr_2I$ and red-emitting (660 nm) $CsPbBr_{0.5}I_{2.5}$ PQDs@glass were ground into powders and appropriately mixed in various ratios. The PL spectra show invariable emission profiles for these four kinds of PQDs with the elongation of storage times (Fig. 4c), yielding stable multi-color luminescence under UV irradiation (Fig. 4d). This result confirms that anion exchange among different glass-stabilized $CsPbX_3$ PQDs can be completely inhibited, which is important for their practical applications in the optoelectronic field.

As a proof-of-concept experiment, the as-prepared $CsPbX_3$ PQDs were demonstrated to be applicable in phosphor-converted light-emitting diodes due to their high PLQYs and superior stability. As evidenced in Fig. S13,† green $CsPbBr_3$ (520 nm), orange $CsPbBr_2I$ (580 nm) and red $CsPbBr_{1.5}I_{1.5}$ (630 nm) PQDs@glass phosphors can be effectively excited after coupling with the commercial InGaN blue chip. Herein, two kinds of prototype lighting devices, *i.e.*, blue-chip/$CsPbBr_3$/$CsPbBr_{1.5}I_{1.5}$ and blue-chip/$CsPbBr_3$/$CsPbBr_2I$/$CsPbBr_{1.5}I_{1.5}$, were constructed. Benefiting from the inhibited anion exchange, stable blue/green/red and blue/green/orange/red emissions can be detected in the electroluminescence (EL) spectra (Fig. 4e and f), yielding white-light luminescence with a tunable correlated color temperature (CCT, 2000–5800 K), color rendering index (R_a, 50–90) and luminous efficiency (LE, 60–93 lm W^{-1}). The extra introduction of orange $CsPbBr_2I$ PQDs contributed to the optimization of R_a and CCT of devices and correspondingly, the emissive color of LED could be tuned from cold white to warm white (insets of Fig. 4e and f). Additionally, controlling the amount of mixed green/orange/red PQD phosphors in the devices enabled the emitting light to move along the black-body radiation locus (Fig. S14 and S15†). It is worth noting that the luminous efficiencies of the present white light-emitting devices (60–93 lm W^{-1}) are comparable or even higher than those of the devices based on chemically synthesized $CsPbBr_3$ and $CsPb(Br/I)_3$ colloidal PQDs (14–61 lm W^{-1}),[45,46] glass-crystallized $CsPbBr_3$ and $CsPb(Br/I)_3$ PQDs (15–61 lm W^{-1}),[35] $CsPbBr_3$ NCs and commercial K_2SiF_6:Mn^{4+} phosphors (63–98 lm W^{-1}),[47,48] $CsPbBr_3$ NCs and $CaAlSiN_3$:Eu^{2+} phosphors (50–60 lm W^{-1})[33] and $CsPbBr_3$/Eu^{3+}/Tb^{3+} co-doped glass (63 lm W^{-1}).[32] This is attributed to the high PLQYs and bright emissions of the present $CsPbBr_3$ and $CsPb(Br/I)_3$ PQDs@glass nanocomposites (Fig. S16†). Importantly, with the increase in the forward bias current, green, orange and red emissions from $CsPbBr_3$, $CsPbBr_2I$ and $CsPbBr_{1.5}I_{1.5}$ PQDs, respectively, were proportionally enhanced

and the color coordinates of the device remained unchanged (Fig. S17†). The results were quite different from those of a previously reported study,[35] where green emission intensity increased much faster than red emission intensity due to the low PLQY of red PQDs@glass.

In summary, fluoride additives were demonstrated to promote the precipitation of whole-family $CsPbX_3$ PQDs inside borosilicate glass. The 3% PLQY of $CsPbCl_3$ PQDs@glass was reported for the first time and the currently highest PLQYs of 50–60% for the glass-stabilized $CsPb(Br/I)_3$ and $CsPbI_3$ orange/red PQDs were obtained. All these colorful $CsPbX_3$ PQDs@glass products showed excellent long-term stability. Specifically, no obvious loss of PL intensity was observed after immersing them in water for up to 30 days and no detrimental anion exchange occurred among different PQDs due to the effective protection of robust inorganic oxide glass. By adopting the mixed green/red or green/orange/red glass-stabilized PQD powders as color converters, cold/warm white light diodes with tunable optoelectronic parameters could be easily achieved. This work exploits a new strategy for preparing high-performance $CsPbX_3$ PQDs and provides an important advancement in exploring their practical applications in lighting and displays.

Conflicts of interest

The authors declare no competing financial interests.

Acknowledgements

This research was supported by the National Natural Science Foundation of China (51572065, 51972060).

References

1 L. Protesescu, S. Yakunin, M. I. Bodnarchuk, F. Krieg, R. Caputo, C. H. Hendon, R. X. Yang, A. Walsh and M. V. Kovalenko, *Nano Lett.*, 2015, **15**, 3692–3696.
2 X. M. Li, Y. Wu, S. L. Zhang, B. Cai, Y. Gu, J. Z. Song and H. B. Zeng, *Adv. Funct. Mater.*, 2016, **26**, 2435–2445.
3 J. Kang and L. W. Wang, *J. Phys. Chem. Lett.*, 2017, **8**, 489–493.
4 A. Swarnkar, R. Chulliyil, V. K. Ravi, M. Irfanullah, A. Chowdhury and A. Nag, *Angew. Chem., Int. Ed.*, 2015, **5**, 15424–15428.
5 D. Q. Chen and X. Chen, *J. Mater. Chem. C*, 2019, **7**, 1413–1446.
6 J. Shamsi, A. S. Urban, M. Imran, L. De Trizio and L. Manna, *Chem. Rev.*, 2019, **119**, 32963348.
7 Q. A. Akkerman, V. D'Innocenzo, S. Accornero, A. Scarpellini, A. Petrozza, M. Prato and L. Manna, *J. Am. Chem. Soc.*, 2015, **137**, 10276–10281.
8 G. Nedelcu, L. Protesescu, S. Yakumin, M. I. Bodnarchuk, M. J. Grotevent and M. V. Kovlenko, *Nano Lett.*, 2015, **15**, 5635–5640.
9 J. Z. Song, J. H. Li, X. M. Li, M. Xu, Y. H. Dong and H. B. Zeng, *Adv. Mater.*, 2015, **27**, 7162.
10 N. Mondal, A. De and A. Samanta, *ACS Energy Lett.*, 2019, **4**, 32–39.
11 Z. Y. Yong, S. Q. Guo, J. P. Ma, *et al.*, *J. Am. Chem. Soc.*, 2018, **140**, 9942–9951.
12 B. Zhuang, Y. Liu, S. Yuan, H. Huang, J. K. Chen and D. Q. Chen, *Nanoscale*, 2019, **11**, 15010–15016.
13 T. Ahmed, S. Seth and A. Samant, *Chem. Mater.*, 2018, **30**, 3633–3637.
14 Y. T. Dong, T. Qiao, D. Kim, D. Parobek, D. Rossi and D. H. Son, *Nano Lett.*, 2018, **18**, 3716–3722.
15 D. D. Yang, X. M. Li, W. H. Zhou, S. Zhang, C. Meng, Y. Wu, Y. Wang and H. B. Zeng, *Adv. Mater.*, 2019, **31**, 1900767.
16 Y. Wei, Z. Y. Cheng and J. Lin, *Chem. Soc. Rev.*, 2019, **48**, 310–350.
17 L. N. Quan, F. P. G. de Arquer, R. P. Sabatini and E. H. Sargent, *Adv. Mater.*, 2018, **30**, 1801996.
18 T. Chiba, Y. Hayashi, H. Ebe, K. Hoshi, J. Sato, S. Sato, Y. J. Pu, S. Ohisa and J. Kido, *Nat. Photonics*, 2018, **12**, 681.
19 K. B. Lin, J. Xing, L. N. Quan, *et al.*, *Nature*, 2018, **562**, 245–248.
20 Q. S. Chen, J. Wu, X. Y. Ou, *et al.*, *Nature*, 2018, **561**, 88–93.
21 M. Lu, X. Y. Zhang, X. Bai, *et al.*, *ACS Energy Lett.*, 2018, **3**, 1571–1577.
22 F. Krieg, S. T. Ochsenbein, S. Yakunin, *et al.*, *ACS Energy Lett.*, 2018, **3**, 641–646.
23 T. Yang, Y. P. Zheng, Z. T. Du, W. N. Liu, Z. B. Yang, F. M. Gao, L. Wang, K. C. Chou, X. M. Hou and W. Y. Yang, *ACS Nano*, 2018, **12**, 1611–1617.
24 M. Liu, G. H. Zhong, Y. M. Yin, J. S. Miao, K. Ki, C. Q. Wang, X. R. Xu and H. Meng, *Adv. Sci.*, 2017, **4**, 1700335.
25 S. Yakunin, L. Protesescu, F. Krieg, M. I. Bodnarchuk, G. Nedelcu, M. Humer, G. De Luca, M. Fiebig, W. Heiss and M. V. Kovalenko, *Nat. Commun.*, 2015, **6**, 8056.
26 J. H. Li, L. M. Xu, T. Want, *et al.*, *Adv. Mater.*, 2017, **29**, 1603885.
27 S. Zou, Y. Liu, J. Li, C. Liu, R. Feng, F. Jiang, Y. Li, J. Song, H. Zeng, M. Hong and X. Chen, *J. Am. Chem. Soc.*, 2017, **139**, 11443–11450.
28 T. Xuan, J. Huang, H. Liu, S. Lou, L. Cao, W. Gan, R. Liu and J. Wang, *Chem. Mater.*, 2019, **31**, 1042–1047.
29 B. Ai, C. Liu, J. Wang, J. Xie, J. J. Han and X. J. Zhao, *J. Am. Ceram. Soc.*, 2016, **99**, 2875–2877.
30 X. X. Di, Z. M. Hu, J. T. Jiang, M. L. He, L. Zhou, W. D. Xiang and X. J. Liang, *Chem. Commun.*, 2017, **53**, 11068–11071.
31 D. Q. Chen, S. Yuan, J. K. Chen, J. S. Zhong and X. H. Xu, *J. Mater. Chem. C*, 2018, **6**, 12864–12870.
32 Y. Z. Cheng, C. Shen, L. Shen, W. D. Xiang and X. J. Liang, *ACS Appl. Mater. Interfaces*, 2018, **10**, 21434–21444.

33 S. Yuan, D. Q. Chen, X. Y. Li, J. S. Zhong and X. H. Xu, *ACS Appl. Mater. Interfaces*, 2018, **10**, 18918–18926.

34 J. T. Jiang, G. Z. Shao, Z. L. Zhang, L. Ding, H. L. Zhang, J. M. Liu, Z. P. Chen, W. D. Xiang and X. J. Liang, *Chem. Commun.*, 2018, **54**, 12302–12305.

35 Y. Ye, W. Zhang, Z. Zhao, J. Wang, C. Liu, Z. Deng, X. Zhao and J. Han, *Adv. Opt. Mater.*, 2019, **7**, 1801663.

36 S. Liu, Y. Luo, M. He, X. Liang and W. Xiang, *J. Eur. Ceram. Soc.*, 2018, **38**, 1998–2004.

37 P. Lin, T. Lin, P. He and D. P. Sekulic, *J. Mater. Sci.*, 2018, **29**, 232–243.

38 G. R. Kumar, C. S. Rao and M. C. Rao, *Optik*, 2018, **170**, 156–165.

39 Y. Yue, C. Shao, S. Kang, F. Wang, X. Wang, J. Ren, D. He, W. Chen and L. Hu, *J. Non-Cryst. Solids*, 2019, **505**, 333–339.

40 A. Ananthanarayanan, G. Tricot, G. Kothiyal and L. Montagne, *Crit. Rev. Solid State Mater. Sci.*, 2011, **36**, 229–241.

41 G. Lakshminarayana, E. M. Weis, B. L. Bennett, A. Labouriau, D. J. Williams, J. G. Duque, M. Sheik-Bahae and M. P. Hehlen, *Opt. Mater.*, 2012, **35**, 117–125.

42 R. E. Youngman and M. J. Dejneka, *J. Am. Ceram. Soc.*, 2002, **85**, 1077–1082.

43 C. G. Lin, C. Rüssel and L. van Wüllen, *J. Phys. Chem. B*, 2019, **123**, 1688–1695.

44 W. J. Mir, A. Swarnkar and A. Nag, *Nanoscale*, 2019, **11**, 4278–4286.

45 H. Huang, B. K. Chen, Z. G. Wang, T. F. Hung, A. S. Susha, H. Z. Zhong and A. L. Rogach, *Chem. Sci.*, 2016, **7**, 5699–5703.

46 C. Sun, Y. Zhang, C. Ruan, C. Y. Yin, X. Y. Wang, Y. D. Wang and W. W. Yu, *Adv. Mater.*, 2016, **28**, 10088–10094.

47 T. T. Xuan, X. F. Yang, S. Q. Lou, J. J. Huang, Y. Liu, J. B. Yu, H. L. Li, K. L. Wong, C. X. Wang and J. Wang, *Nanoscale*, 2017, **9**, 15286–15290.

48 F. Li, Y. Liu, H. Wang, Q. Zhan, Q. Liu and Z. Xia, *Chem. Mater.*, 2018, **30**, 8546–8554.